

Satellite-derived Time for Enhanced Telecom Networks Synchronization: the ROOT Project

*Original*

Satellite-derived Time for Enhanced Telecom Networks Synchronization: the ROOT Project / Pini, Marco; Minetto, Alex; Vesco, Andrea; Berbecaru, DIANA GRATIELA; Miguel Contreras Murillo, Luis; Nemry, Pierre; De Francesca, Ivan; Rat, Benoit; Callewaert, Krel. - ELETTRONICO. - (2021), pp. 288-293. ( 2021 IEEE 8th International Workshop on Metrology for AeroSpace (MetroAeroSpace 2021) Naples (Italy) June 23 - 25, 2021) [10.1109/MetroAeroSpace51421.2021.9511780].

*Availability:*

This version is available at: 11583/2918537 since: 2021-09-20T11:24:11Z

*Publisher:*

Institute of Electrical and Electronics Engineers (IEEE)

*Published*

DOI:10.1109/MetroAeroSpace51421.2021.9511780

*Terms of use:*

This article is made available under terms and conditions as specified in the corresponding bibliographic description in the repository

*Publisher copyright*

IEEE postprint/Author's Accepted Manuscript

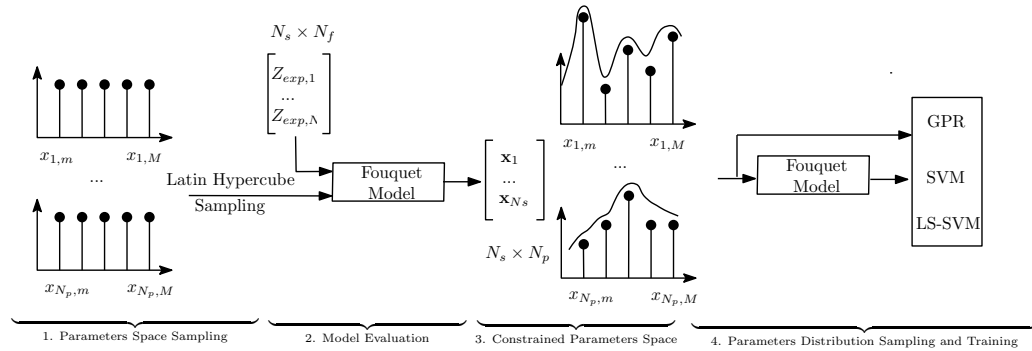
©2021 IEEE. Personal use of this material is permitted. Permission from IEEE must be obtained for all other uses, in any current or future media, including reprinting/republishing this material for advertising or promotional purposes, creating new collecting works, for resale or lists, or reuse of any copyrighted component of this work in other works.

(Article begins on next page)

1 Graphical Abstract

2 **A fast Fuel Cell Parametric Identification approach based on Machine Learning Inverse Models**

3 Antonio Guarino, Riccardo Trincherò, Flavio Canavero, Giovanni Spagnuolo



5 Highlights

6 **A fast Fuel Cell Parametric Identification approach based on Ma-**  
7 **chine Learning Inverse Models**

8 Antonio Guarino, Riccardo Trincherò, Flavio Canavero, Giovanni Spagnuolo

- 9     • Parameter identification of equivalent circuit model performed through  
10       Inverse Model;
- 11     • Parameter search space is first constrained in feasibility regions;
- 12     • Inverse Models built through GPR, SVM and LS-SVM machine learn-  
13       ing regression models;
- 14     • The identification results are shown for both synthetic and experimen-  
15       tal data;
- 16     • Performance and Resource Usage of the embedded implementation are  
17       explored.

18 A fast Fuel Cell Parametric Identification approach  
19 based on Machine Learning Inverse Models

20 Antonio Guarino<sup>a</sup>, Riccardo Trincherò<sup>b</sup>, Flavio Canavero<sup>b</sup>, Giovanni  
21 Spagnuolo<sup>a</sup>

<sup>a</sup>DIEM-University of Salerno, Via Giovanni Paolo II, 132, Fisciano (SA), 84084, Italy

<sup>b</sup>DET-Politecnico di Torino, Corso Duca degli Abruzzi, 24, Torino (TO), 10129, Italy

---

22 **Abstract**

In this paper a computationally efficient optimization approach to the parametric identification of a fuel cell equivalent circuit model is presented. It is based on the inverse model and on machine learning regressions. During the training phase, the inverse model is built numerically by means of advanced regression approaches, i.e., the support vector machine regression, the least squares support vector machine regression and the Gaussian process regression. The training set is synthetically generated to the aim of exploring the parameter space and to characterize different stack operating conditions, including normal and faulty ones. The accuracy of the considered approaches is investigated by employing a test set including many experimental data, consisting of impedance spectra measured through the electrochemical impedance spectroscopy and referring to very different stack operating conditions. The results show that all the considered machine learning methods allow to identify the parameters of the fuel cell model with a low computational burden, so that they fit with the hardware resources of low cost embedded processors. This feature allows to envisage that the proposed approaches are good candidates for a model-based on-line diagnosis of fuel cell stacks.

23 *Keywords:* Parametric identification of Equivalent Circuit Model, Inverse  
24 Model, Machine Learning Regression

---

25 **1. Introduction**

26 Fuel Cells (FCs) and hydrogen-related technologies are a key point of the  
27 European Green Deal and of the Recovery Plan. In order to improve the

28 Life Cycle Assessment (LCA) of FCs' stacks, a significant lifetime has to be  
29 reached. Monitoring and Diagnostic Tools (MDTs) are helpful in evidencing  
30 a malfunctioning and the occurrence of operating conditions that stress the  
31 stack and reduce its Remaining Useful Life (RUL). Although many diagnos-  
32 tic approaches and methodologies are proposed in literature, very often they  
33 employ laboratory measurement systems and/or algorithms requiring signifi-  
34 cant hardware resources. Consequently, their on-line and on-site application  
35 becomes very challenging. At the same time, some efforts are on course to  
36 develop MDTs employing hardware systems and requiring computational ef-  
37 forts that are compatible with FC systems costs, diagnostic accuracy and  
38 time response. For instance, some H2020 funded projects, e.g. [1], have been  
39 aiming at pursuing the objective of having an Electrochemical Impedance  
40 Spectroscopy (EIS) -based MDT using ordinary power electronics and em-  
41 bedded processors to perform frequency domain measurements and detect  
42 a number of faults through on-line diagnostic algorithms. The diagnostic  
43 methods usually work in two spaces: one is the frequency domain, i.e., the  
44 stack impedance spectrum in the Bode or in the Nyquist planes, and the  
45 other is the multidimensional space of the parameters of a suitable non lin-  
46 ear FC stack Equivalent Circuit Model (ECM). The latter requires a robust  
47 approach that takes the impedance spectrum as an input and gives at the  
48 output the set of ECM parameters. This task is quite challenging because of  
49 the number of parameters, of the wide search space and of the lack of a good  
50 guess solution. A further issue is the high non linearity between the function,  
51 which is usually considered as the objective of the optimization problem, e.g.,  
52 the Root Mean Square Error (RMSE) between the ECM impedance and the  
53 experimental data, and the parameters thereof. Some approaches are pro-  
54 posed in literature, e.g. in [2], but they are based on specific assumptions  
55 about the signal-to-noise level affecting the data; consequently, they do not  
56 always ensure the convergence towards the absolute minimum RMSE value  
57 or they have a significant computational burden.

58 Machine learning (ML) has been using more and more in energy problems.  
59 An increasing number of ML-based approaches to monitoring, diagnosis and  
60 RUL prediction of batteries and FCs can be found in the recent literature. In  
61 [3, 4] multiple ML-based approaches have been employed to RUL estimation  
62 of a set of batteries by using charging, discharging, internal resistance and  
63 temperature data. The effectiveness of such approaches that operate on  
64 the battery early usage data is demonstrated. In [5], the battery state of  
65 health is estimated by employing mechanical and electrical features through

66 an Autoencoder and a Gaussian Process Regression (GPR) based estimation  
67 model. In [6, 7] an artificial neural network is used to estimate the remaining  
68 battery capacity. In [8], a number of variables, e.g., stack current and voltage,  
69 air supplier control signal, temperatures, air flow rates, is monitored and their  
70 values are compared with those ones computed through a suitable model.  
71 The patterns of the resulting differences are used to train supervised ML  
72 methods that are then able to classify different faults. In order to ensure  
73 a simultaneous faults detection, instead then addressing independent faults  
74 only, in [9] a deep learning network called stacked sparse autoencoder is  
75 proposed. The stack voltage is also the subject of the study presented in [10]:  
76 some relevant features are extracted and allow ML approaches to identify the  
77 fault.

78 FC degradation prediction in presence of a variable load is performed in  
79 [11] and [12] through a method based on a Genetic Algorithm (GA) and an  
80 Extreme Learning Machine (ELM). The long term dynamic behavior of the  
81 stack voltage is exploited in [13] to predict the performance degradation by  
82 using a Grid Long Short-Term Memory (G-LSTM) Recurrent Neural Net-  
83 work (RNN). A Support Vector Machine (SVM) classifier is adopted in [14]  
84 for detecting FC faults by using a 3D model. The validation of the multi-  
85 scale hybrid degradation index formulated in [15] and of the the approach  
86 aimed at predicting the FC RUL presented in [16] is done through a ML tool  
87 operating on experimental data. Moreover, a ML algorithm has been used  
88 in [17] to find the best trade off between the EIS measurement time and the  
89 fault detection accuracy through the impedance spectrum. The diagnosis is  
90 conducted in the frequency space only, without any parametric identification  
91 process. To this regard, the adoption of ML techniques for system param-  
92 eters identification is quite rare in literature. Few examples refer to dynamical  
93 systems identification: e.g., in [18] the systems considered are described by  
94 differential-algebraic equations and the sum of the squared deviations of the  
95 values of the state vector's coordinates from their exact counterparts obtained  
96 through measurements at different time instants is considered as the objec-  
97 tive function whose value is minimized through the adaptive random search  
98 method. In [19], transfer learning methods are used to address a challenge in  
99 state-space linear parameter-varying model identification and learning. Ker-  
100 nelized ML is adopted when the distributions of the training and testing sets  
101 are different.

102 This paper shows that the parametric identification of a Polymer Elec-  
103 trolyte Membrane (PEM) FC ECM can be effectively performed by using

104 the *inverse model* [20]. A mathematical model, i.e., a multivariate func-  
105 tion, is achieved as first. Then, it exploits a set of experimental EIS spectra  
106 to identify the parameters of the widely recognised ECM presented in [21].  
107 Since the parameters identification is carried out via a straightforward eval-  
108 uation of the inverse model over the experimental values of the EIS spectra,  
109 the proposed approach ensures a good compromise between computational  
110 burden and accuracy, thus a performance that is better than the one the  
111 stochastic identification techniques presented in literature are able to guar-  
112 antee [22][23][24].

113 The construction of the inverse model, which is the core of the proposed  
114 method, is not straightforward. Indeed, the inverse map is usually extremely  
115 non-linear and ill-posed, this meaning that a given EIS spectrum might be  
116 generated by more than one set of the ECM parameters. In order to mitigate  
117 the above issue, in this paper three advanced ML regression methods are  
118 considered. Specifically, the SVM regression [25], the Least Squares SVM  
119 regression (LS-SVM) [26] and the GPR [27] are adopted to construct the  
120 inverse model from synthetic data. The above techniques have been selected  
121 for two main reasons. First of all, they are non-parametric techniques in  
122 which the number of unknowns to be estimated during the model training  
123 is independent from the dimensionality of the input space, i.e., from the  
124 number of frequency points in the EIS spectrum. This allows to minimize  
125 the number of training samples required by the model training and thus the  
126 model complexity. Moreover, the regularizer used by the SVM and LS-SVM  
127 regressions, as well as the noise term in the GPR, can be used to mitigate the  
128 ill-posedness of the inverse model [28, 29]. The proposed approaches have  
129 been also implemented in a low cost embedded system to demonstrate their  
130 on-site and on-line potential; their performance is validated through a large  
131 test set consisting of experimental EIS spectra.

132 The experimental test set has been obtained during the HEALTHCODE  
133 H2020 project [1] on a PEM stack having 46 cells and an active area of 100  
134  $cm^2$ . The stack was tested at  $0.4 A/cm^2$  under different hydrogen and oxygen  
135 utilization and for different humidity levels. The considered dataset refers  
136 to cells number 1, 2, 23, 45, and 46 with measurements performed in the  
137 range from 50 mHz to 2 kHz for a total of 157 spectra. Further details on  
138 the testing procedure and on the study of the impact of water management  
139 and reactant utilization through EIS are disclosed in [30][31].

140 The paper is organized as follows. Section II is aimed at describing the  
141 proposed ML-based identification approach and Section III gives the details

142 of the application of the ML methods adopted. Section IV shows the proce-  
 143 dure used to produce the synthetic data that have been used for the learning  
 144 phase. Sections V and VI provide the analysis of the results based on syn-  
 145 thetic and experimental data, respectively. Section VII shows the results of  
 146 an approach validation performed through an embedded platform that is a  
 147 candidate for the on-line application of the proposed approaches. The com-  
 148 putational burden of the proposed approach in comparison with that one  
 149 of an accurate stochastic approach proposed in literature is also provided.  
 150 Conclusions end the paper.

## 151 2. Gray-Box System Identification via Forward Models

System identification aims at building a mathematical model on the basis  
 of measured data [32]. Given the experimental FC impedance values  $\mathbf{Z}_{exp} =$   
 $[Z_{exp}(f_1), \dots, Z_{exp}(f_{N_f})]^T \in \mathbb{C}^{N_f}$  in a given frequency range, the goal is to  
 identify the optimal configuration  $\mathbf{x}_*$  of the  $N_p = 6$  free parameters  $\mathbf{x} =$   
 $[x_1, \dots, x_{N_p}]^T$  of the Fouquet ECM  $\bar{Z}_F(f; \mathbf{x})$  (see the Appendix and [21] for  
 additional details), such that:

$$Z_{exp}(f) \approx \bar{Z}_F(f; \mathbf{x}_*), \quad (1)$$

152 Literature results allow to assume that the Fouquet model is able to fit, with  
 153 a good accuracy, the experimental spectra.

154 The chosen ECM has a closed-form and it provides a gray-box model, i.e.,  
 155 a model built from a-priori knowledge, for the system identification. The  
 156 Fouquet model is a forward map, or forward model, that for any configuration  
 157  $\mathbf{x}$  of its parameters is able to provide the corresponding impedance value  
 158  $\bar{Z}_F(f; \mathbf{x})$  at the desired frequency value  $f$ .

159 The identification problem (1) can be also formulated by means of an  
 160 objective function whose value has to be optimized through a suitable al-  
 161 gorithm. For instance, the configuration  $\mathbf{x}_*$  can be estimated as the one  
 162 that minimizes the average of the magnitudes of the squared error computed  
 163 between the experimental impedance values collected in  $\mathbf{Z}_{exp}$  and the cor-  
 164 responding ones predicted by the Fouquet model  $\bar{Z}_F$  in a given frequency  
 165 range:

$$\mathbf{x}_* = \arg \min_{\mathbf{x}} \frac{1}{N_f} \sum_{i=1}^{N_f} |Z_{exp}(f_i) - \bar{Z}_F(f_i; \mathbf{x})|^2. \quad (2)$$

166 The properties of such an optimization problem, e.g. its convexity, depend  
 167 on the structure of the forward model  $\bar{Z}_F$ . As an example, the problem at  
 168 hand turns out to be convex when the model  $\bar{Z}_F$  is so simple that it can be  
 169 written as a linear combination of its input parameters  $\mathbf{x}$ . However, such  
 170 minimization problem can be usually classified as a non-convex optimization  
 171 with several local minima [33], which might require advanced optimization  
 172 algorithms, as in [22][23].

173 Alternatively, provided that the candidate model  $\bar{Z}_F(f; \mathbf{x})$  can be inex-  
 174 pensively evaluated for any set of the input parameters  $\mathbf{x}$ , the above optimiza-  
 175 tion problem can be tackled via a grid search approach. It is a brute force op-  
 176 timization scheme, in which the  $N_p$  parameters can be interpreted as uniform  
 177 distributed random variables in a given range (i.e.,  $x_i \sim \mathcal{U}(x_{i,min}, x_{i,max})$ ),  
 178 then the model  $\bar{Z}_F(f; \mathbf{x})$  is evaluated for a large number of realizations of the  
 179 input random parameters drawn according to their probability distribution  
 180 functions (PDFs). Thus, the optimal parameters set  $\mathbf{x}_*$  can be estimated  
 181 among all the considered realizations as the one that minimizes the cost  
 182 function of the optimization problem (2). This approach is straightforward  
 183 and does not require to calculate the gradient function of the cost function,  
 184 but it turns out to be quite cumbersome and computational expensive. In  
 185 fact, the accuracy and the reliability of optimal solution  $\mathbf{x}_*$  predicted by such  
 186 brute force approach heavily depends on the number of calls to the model  
 187  $\bar{Z}_F$ , and thus on the number of realizations of the random variables  $\mathbf{x}$  con-  
 188 sidered during the optimization process. This limits the online use of such  
 189 an approach through embedded systems.

### 190 3. Inverse Model for System Identification

191 The inverse model approach presented in this paper is an effective candi-  
 192 date for the FC ECM identification [20].

The inverse model denoted as  $\mathcal{M}^{-1}$  goes in the opposite direction with  
 respect to forward model  $\bar{Z}_F(f; \mathbf{x})$  used in the conventional optimization  
 approach (2); it is:

$$\mathbf{x}_* = \mathcal{M}^{-1}(\mathbf{Z}_{exp}), \quad (3)$$

193 where, the vector  $\mathbf{x}_* \in \mathbb{R}_p^N$  collects the identified system parameters,  $\mathbf{Z}$  is  
 194 a vector collecting the experimental impedance values evaluated at the fre-  
 195 quency  $\mathbf{f} = [f_1, \dots, f_{N_f}]^T$  and the inverse map  $\mathcal{M}^{-1} : \mathbb{C}^{N_f} \rightarrow \mathbb{R}^d$ .

196 Specifically, starting from the experimental impedance values  $\mathbf{Z}_{exp}$ , the  
 197 inverse map  $\mathcal{M}^{-1}$  is able to directly provide, without requiring to solve any  
 198 optimization problem or to use an iterative algorithm, the optimal configu-  
 199 ration of the ECM parameters  $\mathbf{x}_*$ . Indeed, by means of the inverse model,  
 200 the identification task becomes as simple as a trivial function evaluation.

201 Unfortunately, for realistic cases in which the inverse map cannot be  
 202 computed explicitly from the forward one, the construction of the inverse  
 203 model is rather challenging. First of all, even if a mathematical relationship  
 204 for the forward model is known, the inverse model might not be available  
 205 in a closed-form. In such cases, the model must be constructed numerically  
 206 with the help of regression or interpolation techniques, starting from a set of  
 207 experimental and/or synthetic training data provided by the forward model.  
 208 Moreover, inverse models are often ill-posed, since they can lead to a one-to-  
 209 many map (i.e., the inverse model turns out to be a non-injective function),  
 210 in the sense that a given set of value of the model output might be generated  
 211 by more than one combinations of the system parameters.

212 Advanced ML regression techniques are promising candidates for building  
 213 an accurate approximation of the inverse map in a high dimensional space. In  
 214 this paper, the effectiveness of three ML regressions, i.e., SVM regression [25],  
 215 LS-SVM regression [26] and the GPR [27], is investigated.

### 216 3.1. SVM and LS-SVM regression

Let us consider the problem of constructing the inverse map  $\mathcal{M}^{-1}$ , start-  
 ing from a set of  $N_s$  training samples  $\mathcal{D} = \{(\mathbf{x}_l, \mathbf{y}_l)\}_{l=1}^{N_s}$ , in which the vector  
 $\mathbf{x}_l \in \mathbb{R}^{N_p}$  collects the training realizations of the system parameters and  
 $\mathbf{y}_l = [\text{Re}\{Z_{1,l}\}, \dots, \text{Re}\{Z_{N_f,l}\}, \text{Im}\{Z_{1,l}\}, \dots, \text{Im}\{Z_{N_f,l}\}]^T \in \mathbb{R}^{2N_f}$  is a real  
 value vector collecting the corresponding real and imaginary parts of the FC  
 impedance values, the latter being synthetic or experimental data. The pri-  
 mal space formulation of the inverse model  $\tilde{\mathcal{M}}_i^{-1}$  for  $i$ -th component of the  
 parameter vector  $\mathbf{x}$  built via the SVM and LS-SVM regression, writes [25, 26]:

$$x_i \approx \mathcal{M}_i^{-1}(\mathbf{y}) = \langle \mathbf{w}_i, \phi(\mathbf{y}) \rangle + b_i \quad (4)$$

217 where  $\phi : \mathbb{R}^{N_p} \rightarrow \mathbb{R}^D$  is a vector collecting  $D$ -basis functions <sup>1</sup>,  $\mathbf{w}_i \in \mathbb{R}^D$  is a  
 218 vector collecting the regression unknowns and  $b_i$  is the bias term. The above  
 219 formulation can be repeated to model all the components of the vector  $\mathbf{x}$ .

---

<sup>1</sup>For the sake of simplicity, it has been assumed that all the components of parameter  
 vector  $x_i$  share the same basis functions.

For the LS-SVM and SVM regressions, the unknowns (i.e.,  $\mathbf{w}_i$  and  $b_i$ ) are estimated by solving the following optimization problem:

$$\min_{\mathbf{w}_i, b_i} \frac{1}{2} \|\mathbf{w}_i\|_{L_2}^2 + \gamma_i \sum_{l=1}^{N_s} \ell(x_{i,l}, \langle \mathbf{w}_i, \phi(\mathbf{y}_l) \rangle + b_i) \quad (5)$$

where  $\ell(\cdot)$  is a cost function proving the error of the model on the training samples. This means that the coefficients  $\mathbf{w}_i$  and the bias term  $b_i$  are estimated by minimizing the average of the cost function evaluated between the training data and the model predictions penalized by a L2 regularizer (i.e.,  $\|\mathbf{w}_i\|^2$ ). The latter term adds a penalty to the model accuracy on the training samples, thus mitigating the detrimental effects of the ill-posed problem and also reducing overfitting [34]. The effect of the regularizer in the optimization problem in (5) is tuned by the hyperparameter  $\gamma_i$ , usually estimated via cross-validation (CV) during the model training. A squared loss function is used as cost function for the LS-SVM regression<sup>2</sup>, whereas the SVM regression uses the  $\varepsilon$ -insensitive loss function. Interested readers can refer to [25] for additional details.

It is important to notice that the primal space formulation of the LS-SVM and SVM regression provides a parametric model, in which the number of unknowns to be estimated (i.e., the cardinality of the vector  $|\mathbf{w}| = D$ ) is equal to the number of basis functions considered in the liner expansion in (4). This means that the obtained model suffers the curse of dimensionality (i.e., a reduction of the model efficiency when either the model complexity and the number of parameters increases).

The dual formulation available for the LS-SVM and SVM regression allows mitigating the above issue and writes:

$$x_i = \sum_{l=1}^{N_s} \alpha_{i,l} k(\mathbf{y}, \mathbf{y}_l) + b_i, \quad (6)$$

where the coefficients  $\alpha_{i,l}$  and the bias term  $b_i$  are estimated by the regression algorithm during the training process and  $k(\cdot, \cdot) : \mathbb{R}^{2N_f \times 2N_f} \rightarrow \mathbb{R}$  is the kernel function defined as the inner product of between the basis function vectors, i.e.,  $k(\mathbf{y}, \mathbf{y}_l) = \langle \phi(\mathbf{y}), \phi(\mathbf{y}_l) \rangle$ . Thanks to the kernel function  $k(\cdot, \cdot)$ , the dual

---

<sup>2</sup>For mathematical convenience, in the LS-SVM regression the squared loss function is multiplied by a constant term 1/2.

243 space formulation in (6) does not require an explicit definition of the basis  
 244 functions  $\phi(\mathbf{y})$ . This is the so-called “kernel trick” [25]. Several kernel func-  
 245 tions with different mathematical properties and features are available [35].  
 246 The most common ones are:

- 247 • linear kernel:  $k(\mathbf{y}, \mathbf{y}_l) = \mathbf{y}^T \mathbf{y}_l$ ;
- 248 • polynomial kernel of order  $q$ :  $k(\mathbf{y}, \mathbf{y}_l) = (1 + \mathbf{y}^T \mathbf{y}_l)^q$ ;
- 249 • Gaussian radial basis function (RBF) kernel:  $k(\mathbf{y}, \mathbf{y}_l) = \exp(-\|\mathbf{y} - \mathbf{y}_l\|^2/2\sigma^2)$ ,  
 250 where  $\sigma$  is the kernel hyperparameter.

251 Hereafter, in this paper the Radial Basis Function (RBF) kernel will be  
 252 adopted, since it has shown an excellent performance in high nonlinear re-  
 253 gression problems [25, 28].

254 In the above dual formulation of the SVM and LS-SVM regression, the  
 255 number of regression unknown  $\alpha_{i,l}$  turns out to be independent from the di-  
 256 mensionality of the input space (i.e., the cardinality of  $\mathbf{y}$ ). This is extremely  
 257 useful to overcome the curse-of-dimensionality issue. Moreover, the regular-  
 258 izer used in the primal space formulation allows us to mitigate the ill-posed  
 259 problem resulting from the inverse map.

260 It should also be noted that the unknowns of the dual form of the LS-  
 261 SVM formulation can be suitably estimated as a solution of a linear problem  
 262 by inverting a square matrix [26]. On the other hand, due to the  $\varepsilon$ -insensitive  
 263 loss function, the convex optimization problem for the case of the SVM leads  
 264 to a sparse solution, but it must be solved numerically [25].

### 265 3.2. GPR Regression

Differently from the LS-SVM and SVM regression, the GPR can be used  
 to build a probabilistic version of the inverse surrogate model. Starting from  
 the  $N_s$  training samples  $\mathcal{D} = \{(\mathbf{x}_l, \mathbf{y}_l)\}_{l=1}^{N_s}$ , the GPR allows to train a prob-  
 abilistic inverse model able to estimate for any configuration of the input  
 parameters a statistical interpretation of its prediction in terms of a Gaus-  
 sian distribution, which provides additional information on its reliability [27].  
 Specifically, for any test sample  $\mathbf{y}_*$ , the output of a GPR model is:

$$x_{i,*} \sim p(x_{i,*} | \mathbf{y}_*, \mathcal{D}) = \mathcal{N}(\mu_{\mathbf{y}_*}, \sigma_{\mathbf{y}_*}^2) \quad (7)$$

in which  $\mu_{\mathbf{y}_*}$  and  $\sigma_{\mathbf{y}_*}^2$  are the so-called posterior mean and variance, computed as follows:

$$\mu_{\mathbf{y}_*} = \mathbf{k}_*^T (\mathbf{K} + \sigma_n^2 \mathbf{I})^{-1} \mathbf{x} \quad (8)$$

$$\sigma_{\mathbf{y}_*}^2 = k_{**} - \mathbf{k}_*^T (\mathbf{K} + \sigma_n^2 \mathbf{I})^{-1} \mathbf{k}_* \quad (9)$$

where  $\mathbf{y} = [y_1, \dots, y_{2N_f}]$ ,  $\mathbf{K} \in \mathbb{R}^{N_s \times N_s}$  is the correlation matrix in which the covariance function  $k$  is evaluated on pairs of the training data (i.e.,  $K_{ij} = K(\mathbf{y}_i, \mathbf{y}_j)$ ),  $\mathbf{k}_* = [k(\mathbf{y}_1, \mathbf{y}_*), \dots, k(\mathbf{y}_L, \mathbf{y}_*)]^T$  is a column vector,  $k(\mathbf{y}_*, \mathbf{y}_*)$  is a scalar,  $\mathbf{I} \in \mathbb{R}^{N_s \times N_s}$  is the identity matrix and  $\sigma_n^2$  is an hyperparameter representing the variance of a possible additive noise corrupting the training dataset. Similarly to the kernel function, the covariance function used in the GPR defines the correlation between the values of pairs of model output at different point in the parameters space. Hereafter in this paper, a squared exponential covariance function, also known as RBF kernel, is used for the GPR, i.e.,  $k(\mathbf{y}, \mathbf{y}') = \exp(-\|\mathbf{y} - \mathbf{y}'\|^2 / 2\sigma_l^2)$  [27], where  $\sigma_l$  is a hyperparameters estimated during the model training.

#### 4. Learning framework for the inverse model

The LS-SVM, the SVM and the GPR regression models learn the inverse model through a suitable framework. To learn the inverse function of the Fouquet model through a data-driven regression technique, it is necessary to observe both the domain and the co-domain of the function  $\mathbf{x} = \mathcal{M}^{-1}(\mathbf{y})$ . However, given the very high dimensionality of the two spaces, one depending on the number of frequencies, the other on the number of parameters, an unconstrained generation of observations would be computationally intractable. It is worth to note that, since the forward model  $\bar{\mathbf{Z}} = \bar{Z}_F(\mathbf{x}, \mathbf{f})$  is available, the sampling can be limited to the parameters space and the spectrum obtained through the evaluation of the direct model for each sampled parameters' set. However, even in this case, the training procedure would benefit from a bounded search space. From a computational perspective, bounding the parameters values between specific maxima and minima values drastically reduce the training time. Additionally, from a physical perspective, only certain combinations of parameters are feasible and lead to a meaningful impedance spectra, thus only certain regions of the parameters space are worth to be explored.

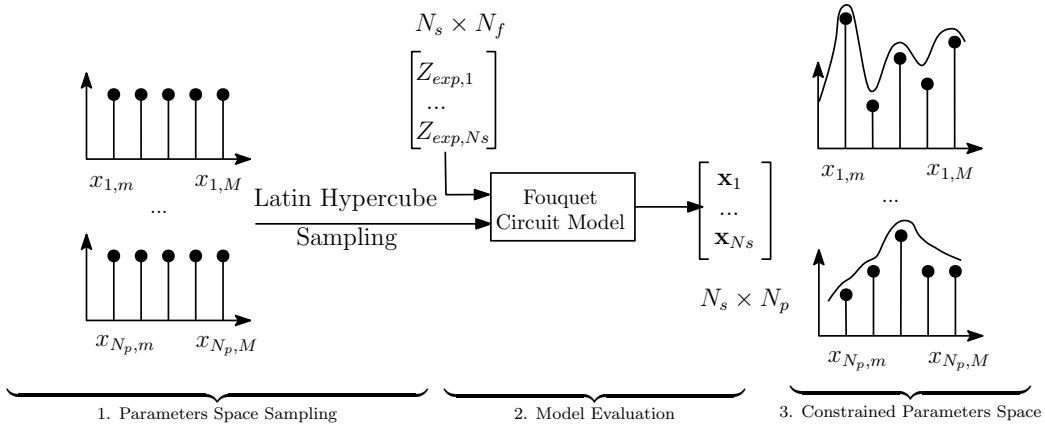


Figure 1: Generation of the training set. Each set of parameters is sampled through the LHS method and is processed with the Fouquet model in the Grid Search Procedure.

295 A synthetic dataset, which is obtained through a specific data-generating  
 296 procedure shown in Fig. 1, has been employed for training purposes. It em-  
 297 ploys the grid search optimization briefly described in Sec. 2 together with  
 298 the Fouquet ECM in which the candidate sets of parameters are sampled  
 299 from the search space via a Latin Hypercube Sampling (LHS) scheme. In  
 300 the figure,  $N_s$  refers to the number of training samples,  $N_p = 6$  is the num-  
 301 ber of parameters involved in the Fouquet ECM, i.e. the dimension of the  
 302 parameters vector  $\mathbf{x}$ , and  $N_f = 48$  is the number of frequency values.

#### 303 4.1. Parameters Space Sampling

304 Fig. 1 shows that, at the beginning of the procedure, the parameters  
 305 space is sampled in the range between  $\mathbf{x}_m$  and  $\mathbf{x}_M$ . These limits have been  
 306 set after having analysed the experimental impedance spectra corresponding  
 307 to the extreme fault conditions. Indeed, the experimental data have been  
 308 obtained by inducing stack faults with an increasing level of severity. By  
 309 moving the stack operating condition away from the nominal one, impedance  
 310 modulus and phase change and lead to visible effects on the spectra, e.g. in  
 311 terms of a magnification or reduction of the arcs in the Nyquist diagram.  
 312 The effect depends on the specific fault, on its severity, and on the duration  
 313 of the fault condition. For a specific operating condition imposed at stack  
 314 level, the spectra of its cells that are connected in series may not exhibit the  
 315 same alteration, because of inhomogeneities in the gas flows, constructive  
 316 mismatching among cells and differences in cells degradation rate.

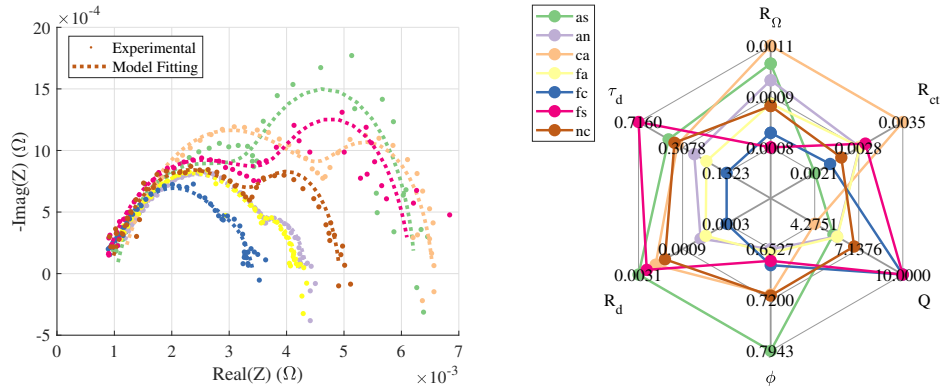


Figure 2: EIS Impedance curves (top panel) in nominal and faulty conditions identified offline and the corresponding parameters (bottom panel) defining the parameters space.

317 Thus, the boundaries for each parameter range have been fixed by picking,  
 318 in a subset of curves referring to the same operating condition, the spectrum  
 319 that is the farthest from the nominal one. The resulting spectra are consid-  
 320 ered as extreme ones and selected for a robust identification. The parametric  
 321 identification has been performed according to the approach described in [36].

322 The fluctuation of the experimental measurements around the GA-based  
 323 identified impedance curve is shown in Fig. 2. In the figure, the curves refer  
 324 to the fitting while the dots are the EIS measurements of the farthest curves  
 325 from the reference. Among the selected curves, the extreme values of each  
 326 parameter are considered. Fig. 2 also shows the coverage of the parameters  
 327 space obtained through the described procedure, together with the obtained  
 328 identified parameters set for each specific operating condition. The colors  
 329 are used to distinguish the different FC working conditions: Air Starvation  
 330 (*as*), Anode and Cathode Drying (*an* and *ca*), Anode and Cathode Flooding  
 331 (*fc* and *fa*) Fuel Starvation (*fs*) and Normal Conditions (*nc*).

#### 332 4.2. Grid Search Optimization and the reduced parameters space

333 The parameters space defined in the previous subsection and depicted  
 334 in Fig. 1 with the left-most stem plot, is sampled through a LHS proce-  
 335 dure and evaluated during the grid search optimization to obtain the set  
 336 of solutions  $\mathbf{X}_{MC} = [\mathbf{x}_1, \dots, \mathbf{x}_{N_s}]$  for the experimental impedance spectra  
 337  $[\mathbf{Z}_{exp,1}, \dots, \mathbf{Z}_{exp,N_s}]$ . Thereby, the set of solutions  $\mathbf{X}_{MC}$  is used to reduce the  
 338 initial parameters space and build a prior discrete  $N_p$ -dimensional distribu-  
 339 tion of the parameters. This is represented by the rightmost stem plot in

340 Fig. 1. The obtained discrete distribution is smoothed with a Kernel Density  
341 Estimate (KDE) procedure so that it can be sampled to obtain an expanded  
342 training set of arbitrary dimension [37]. This procedure ensures that the  
343 three regression algorithms are focused on the plausible regions of the pa-  
344 rameters space, which are those ones leading to impedance spectra that are  
345 representative of the FC operating conditions. Moreover, the availability of a  
346 continuous distribution from which an arbitrary number of spectra is drawn,  
347 allows to benchmark the performance of the regression algorithms by using  
348 different sizes of the training set.

## 349 5. Results on synthetic data

350 The proposed approaches are firstly validated by using the synthetic  
351 dataset. Both the training and test sets are sampled from the reduced pa-  
352 rameters' space that is obtained as it has been described in Section 4.2. The  
353 reduced parameters' space is obtained by using the 30% and 70% of the  
354 experimental spectra, in order to create the training and the testing sets  
355 respectively. Thus, at this stage, the fractions of the experimental dataset  
356 reported above are exploited to estimate the parameters' distributions. The  
357 resulting distributions for the training and test sets are then sampled and  
358 processed through the Fouquet ECM to obtain the corresponding synthetic  
359 impedance spectra that are used for training and test purposes.

360 The use of spectra that do not come from experimental measurements  
361 but that have been generated by using the Fouquet ECM allows to analyse  
362 the performance of the regression algorithms. Indeed, to each synthetic spec-  
363 trum, belonging either to the training set or to the test set, corresponds a set  
364 of parameters of the Fouquet ECM that guarantees the perfect fitting of the  
365 spectrum thereof. Consequently, modelling inaccuracies of the Fouquet ECM  
366 for the available experimental data do not affect the identification result and  
367 the performance of the regression approaches can be analysed in detail. The  
368 use of synthetic data also allows to study the impact of the number of train-  
369 ing samples and of the noise affecting the data in the Nyquist plane, the  
370 latter being added through a simple numeric procedure applied to the test  
371 set. The noise has been added to the smooth impedance generated through  
372 the Fouquet ECM. The spectroscopy measurements are known to be affected  
373 by a stochastic noise, whose standard deviation is a function of the frequency  
374 and the magnitude of the impedance vector [38]. Therefore, to mimic the

375 noise of the available experimental spectra, the impedance used to build the  
 376 synthetic test set has been altered according to (10):

$$Z(f) = \bar{Z}_F(f; \mathbf{x}_*) + \underbrace{(\beta_{re}(f) + j\beta_{im}(f))}_{n(f)}, \quad (10)$$

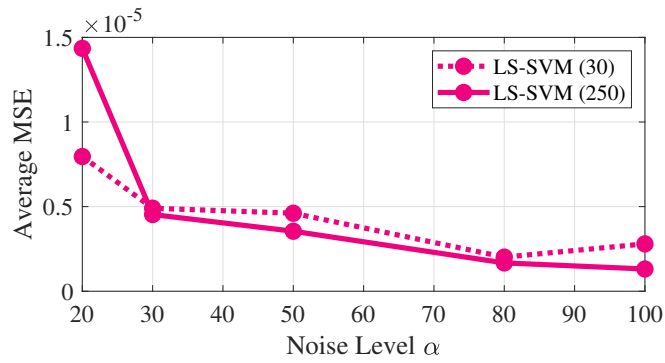
377 where  $\beta_{re}(f), \beta_{im}(f) \sim \mathcal{N}(0, \sigma^2(f))$  are Gaussian distributed stochastic vari-  
 378 ables describing a non-stationary additive noise  $n(f)$ , in which the standard  
 379 deviation is computed according to (11):

$$\sigma(f) = \frac{|\bar{Z}_F(f; \mathbf{x}_*)|}{\alpha} \quad (11)$$

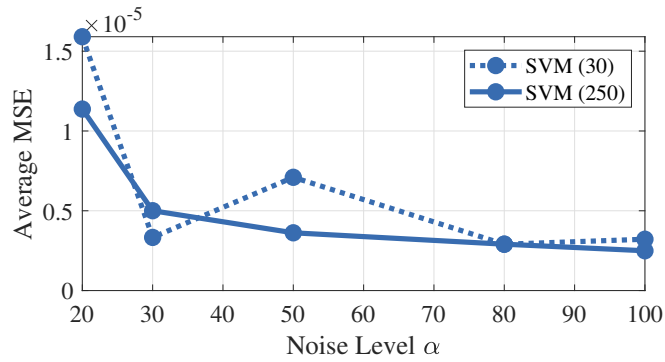
380 and  $\alpha$  is used to change the noise level.

381 The amplitude of the noise term  $n(f)$  is proportional to the impedance  
 382 modulus, and affects its real and imaginary parts independently.

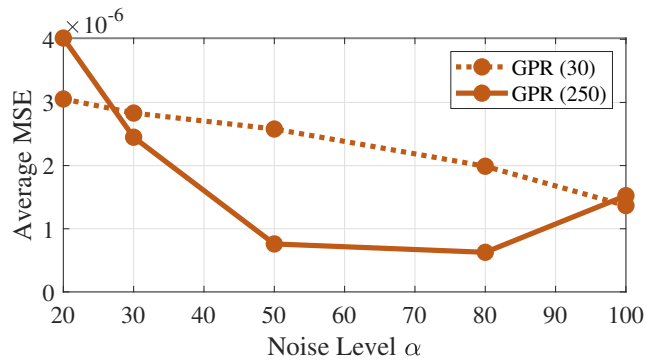
383 Fig. 3 shows the average performance, over three consecutive runs, of  
 384 the three algorithms on the test set. The algorithms are trained to infer  
 385 the vector of parameters  $\mathbf{x}_*$  starting from the impedance  $Z$ . The evaluation  
 386 of the Fouquet model returns the estimated impedance  $\bar{Z}_F(f)(f; \mathbf{x}_*)$ . The  
 387 average MSE norm between the estimated spectra and the ones of the test  
 388 set is used to compare the results. In Fig. 3(a) the LS-SVM performance  
 389 underlines the impact of the noise level for two different sizes of the training  
 390 set. For high levels of noise, thus  $\alpha$  lower than 30, the average performance  
 391 with 250 samples is worst than the one obtained with the reduced sample size  
 392 of 30. When the noise level decreases, the impact of the increased dataset size  
 393 becomes visible. At  $\alpha = 100$  the performance index is halved. Similar results  
 394 are also obtained for the GPR model (Fig. 3(c)) and very similar results  
 395 between the two dataset dimensions have been reached when considering  
 396  $\alpha = 100$ . It follows that, with the proposed parameters space sampling, the  
 397 impact of a reduced training set size is marginal and the size of the training  
 398 set becomes important only for low levels of noise.



(a)



(b)



(c)

Figure 3: Influence of the number of training samples and of noise level  $\alpha$  on the average MSE computed on the synthetic test set: (a) LS-SVM (b) SVM (c) GPR. Each point is the average of three training runs.

399 *5.1. Hyperparameters optimization*

400 For the SVM and the LS-SVM regressions, the optimization of the model  
401 hyperparameters is performed through a 10-fold CV [34] scheme and a Bayesian  
402 optimization [39]. Whilst, the GPR hyperparameters are optimized by max-  
403 imizing the likelihood on the training set via a grid search approach. The  
404 above implementations automate the parameters tuning procedure, thus en-  
405 abling the applicability of the methods to different ECMs with small changes,  
406 often outperforming the standard hand-tuning approaches. The procedure  
407 is executed on the hyperparameters domain defined as it follows. For the  
408 SVM and the LS-SVM these are defined in the range  $C : (1 \times 10^{-6}, 5 \times 10^4)$ ,  
409  $\gamma : (1 \times 10^{-6}, 5 \times 10^4)$  and  $\varepsilon : (1 \times 10^{-11}, 1 \times 10^2)$  (only tuned for the SVM re-  
410 gression). For The GPR, the hyperparameters' ranges are  $\sigma_l : (1 \times 10^{-5}, 1 \times 10^5)$   
411 and  $\sigma_n^2 : (1 \times 10^{-5}, 1 \times 10^5)$ .

412 **6. Experimental Results**

413 The described procedure has been tested on an experimental dataset [1]  
414 described in the Introduction. The parameters space is built by using the  
415 procedure described in the previous section and the grid search optimization  
416 is employed to narrow the search space operating on 70% of the dataset,  
417 corresponding to 110 impedance spectra, while 30% of the set is left for the  
418 results evaluation. The histogram plots shown in Fig. 4 give a comprehensive  
419 view of the obtained results in terms of the MSE resulting by the comparison  
420 of the experimental data with the Fouquet impedance at the same frequency  
421 values. The MSE is obtained by using the parameters sets that are inferred  
422 by the three regression algorithms on all the spectra of the testing set. Af-  
423 ter, for each inferred parameters set, the Fouquet impedance is computed  
424 and the MSE is calculated with respect to the corresponding experimental  
425 data. Consequently, the MSEs histograms shown in Fig. 4 summarize the  
426 performance of the three approaches on all the spectra of the test set. Tab. 1  
427 reports the identification results in terms of mean, median, and interquartile  
428 range (IQR) of the MSE and MAPE calculated over the spectra belonging to  
429 the test set. The mean is reported as an overall performance index and the  
430 median is provided to quantify the robustness of the result over the entire  
431 test set. The closer the mean and median values the better the identification  
432 performance. In this case, the error histogram approaches a normal distri-  
433 bution, indicating that there are no reconstructed spectra with an error that

Table 1: Mean, Median, and Interquartile Range (IQR) of the MSE and MAPE computed on the whole test set

	MSE ( $\times 10^{-5}$ )			MAPE		
	Mean	Median	IQR	Mean	Median	IQR
<b>GPR</b>	0.3179	0.2419	0.2017	0.9985	0.9858	0.0358
<b>SVM</b>	0.3403	0.2325	0.2109	1.0875	1.0844	0.0492
<b>LS-SVM</b>	0.7387	0.5537	0.5407	1.0863	1.0779	0.0438

434 differs significantly from the mean. The interquartile range is also provided  
 435 to assess the variability of the obtained result.

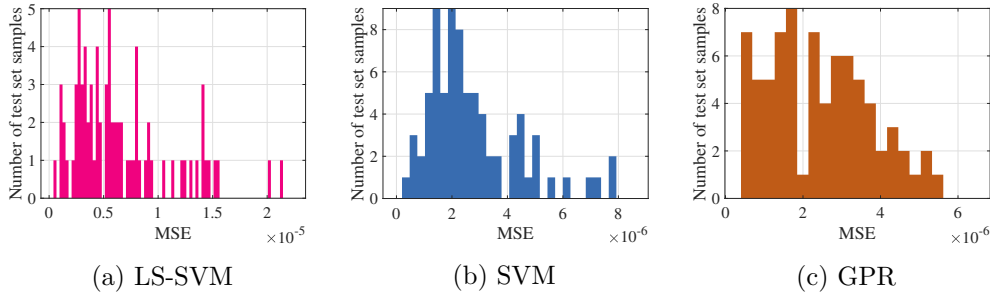


Figure 4: Histogram of the MSE errors computed between the inverse model reconstructions of the impedance spectra and the experimental measurement of the testing set. Each bar corresponds to the number of spectra of the test set giving an MSE falling in the corresponding range.

436 The GPR regression, for a larger number of test set spectra, gives a  
 437 smaller error, both in comparison with those ones ensured by the other meth-  
 438 ods. Moreover, the reduced spread of the values of the histogram plot indic-  
 439 ates that the obtained performance is well generalized on the whole test  
 440 set. The SVM shows an average performance similar to the GPR but with  
 441 an increased spread of the error histogram. Contrarily, the LS-SVM shows a  
 442 performance degradation and higher variability of the result. It is important  
 443 to point out that the low performance of the LS-SVM regression could be  
 444 due to the quite large range of variation the hyperparameters explored during  
 445 the training phase. To quantify the results, different degrees of performance  
 446 have been considered.

447 Experimental EIS spectra are affected by an evident noise and artifacts,  
 448 thus those ones resulting with an error below  $2 \times 10^{-6}$  are considered as  
 449 correctly identified. Fig. 4 shows that GPR and SVM guarantees that the

450 45% and the 41%, respectively, of the spectra in the test set are very well  
 451 identified, because the error keeps below the defined threshold. The LS-  
 452 SVM gives a 10% of the spectra that are identified with an error due to noise  
 453 artifacts. The identification performance is reported in Fig. 5. In both the  
 454 cases, the GPR and SVM spectra show optimal results with an MSE below  
 455  $2 \times 10^{-6}$ . The results shown in Fig. 5(a) and (b) are obtained through LS-  
 456 SVM and are reconstructed with an error equal to  $2.8 \times 10^{-6}$  and  $1.5 \times 10^{-5}$ ,  
 457 respectively.

458 Also, the range  $2 \times 10^{-6} < \text{MSE} < 2.5 \times 10^{-6}$  is giving valuable solutions.  
 459 For the GPR, SVM and LS-SVM models, respectively 11% and 14% and 4%  
 460 of the test set are reconstructed with this error. An example of the quality  
 461 of the reconstruction obtained in this range is shown in Fig. 6.

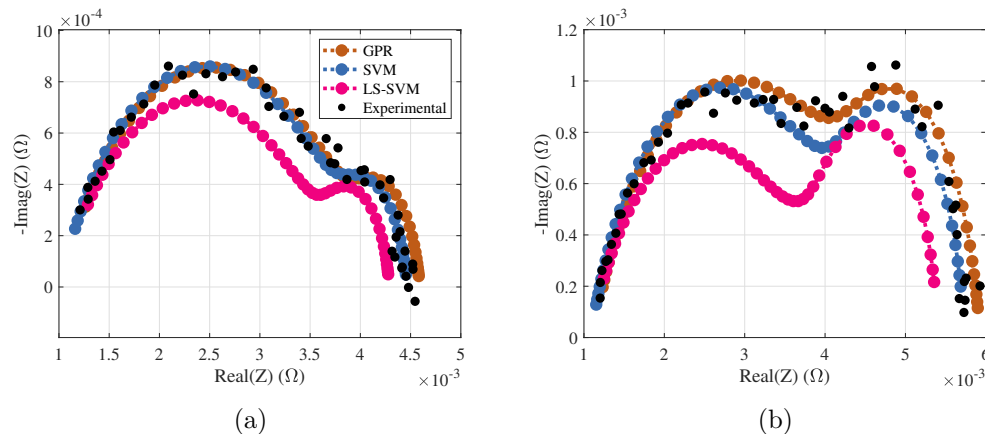


Figure 5: Best identification performance obtained by the GPR and SVM inverse models.

## 462 7. On Field Results

463 An important point of strength of the proposed inverse model is the short  
 464 execution time observed during the phase of inference. Although the training  
 465 is computationally expensive due to the dimensionality of the space to be ex-  
 466 plored and due to the automatic hyperparameters tuning, the trained model  
 467 consists of a simple function, whose evaluation on the measured impedance  
 468 spectra returns the set of parameters. For this reason, differently from other  
 469 standard model identification procedures relying on iterative algorithms, the  
 470 inference through the inverse model is a good candidate for the implemen-  
 471 tation on a low cost embedded system, since the impact on the resources

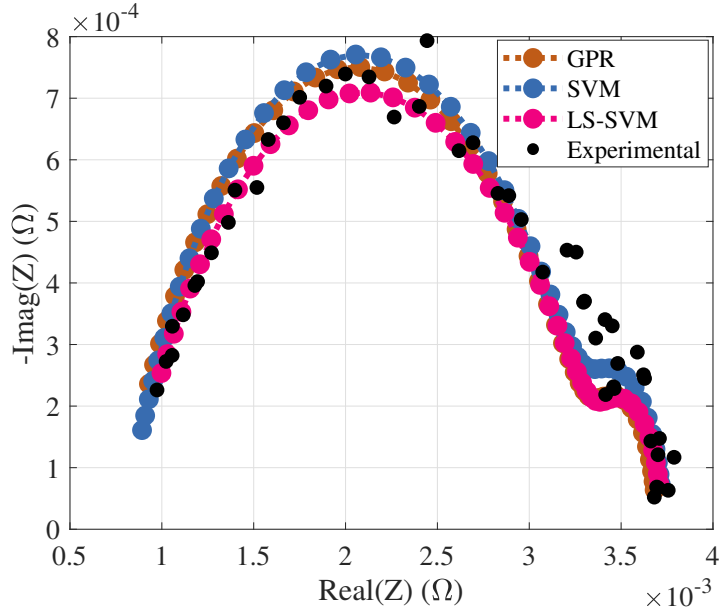


Figure 6: Middle quality identification obtained by the three inverse models.

472 usage is negligible and the execution time is deterministic. Both the later  
 473 aspects are in favor of the approach proposed in this paper with respect  
 474 to any stochastic optimization procedure for parameters identification [22, 23, 40, 41, 42].  
 475 The three algorithms are implemented in Python and executed in a decentralized way.  
 476 The training procedure, that is computationally expensive due to the hyperparameters  
 477 optimization procedure, is executed on the cloud by employing the Google Colab platform.  
 478 The remote machine is equipped with a Dual-Core Haswell Intel Xeon processor at 2.30  
 479 GHz and 12 GB of RAM. After the training procedure, the testing is executed on a  
 480 Raspberry Pi 3 embedded system equipped with a Quad-Core 1.2 GHz Broadcom BCM2837  
 481 CPU and 1 GB of RAM and the execution times of the three algorithms have been  
 482 considered as benchmark. In Fig. 7(a), the training time of the three models is  
 483 reported as a function of the size of the training set. The training time is not only  
 484 affected by the number of samples in the training set, but also by the number of  
 485 hyperparameters to be tuned and the optimization scheme. This explains the scale  
 486 difference between the three techniques. In fact, the training of the SVM regression  
 487 turns out to be the most expensive one, since it requires the tuning of three

490 hyperparameters via the CV. On the other hand, the training is faster for  
 491 the GPR because the optimization of the hyperparameter is carried out on  
 492 the training samples directly, without requiring to compute the CV error.  
 Fig. 7(b) reports the execution time for the inference of a set of parameters.

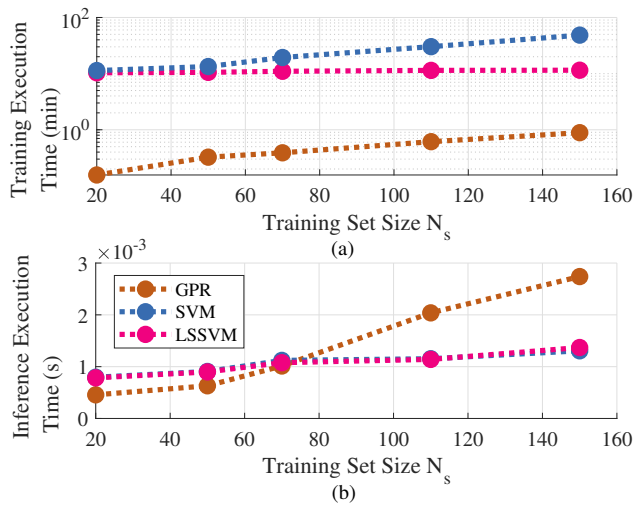


Figure 7: Training (a) and inference (b) execution times of the three regression algorithms.

493 The results clearly highlight the impact of the dimensionality of the training  
 494 set on the inference time. Indeed, for the considered approaches, the model  
 495 complexity increases with the number of training samples considered during  
 496 the model training. The three algorithms infer the parameters set in few  
 497 milliseconds. The chosen regressions trained with 110 samples perform the  
 498 inference in 2 milliseconds for GPR and in slightly above 1 millisecond for  
 499 the SVM and the LS-SVM models, respectively.  
 500

501 It is worth to have a comparison in terms of computation time also with  
 502 approaches based on parameters identification from EIS data through the  
 503 minimization of an objective function value [22][23][43][40]. The objective  
 504 function is computed by fixing a set of Fouquet ECM parameters and a set  
 505 of frequencies, then evaluating the Fouquet impedance and computing the  
 506 MSE between the generated impedance and the experimental data. This  
 507 computation has been performed in Python, like the other inverse models  
 508 solutions, and run on the same Raspberry Pi 3 mentioned above. The average  
 509 execution time is equal to 0.7 ms. This means that a competitive optimization

510 algorithm should be able to find the solution in less than 3 iterations to have  
 511 an execution time that is comparable with that one of the GPR inference  
 512 time, which is slightly above 2ms.

## 513 8. Conclusions

514 Machine learning regression models demonstrated to be an efficient choice  
 515 to solve the inverse problem with minimal and deterministic execution time  
 516 reported during inference. Leveraging the a priori knowledge on the ranges  
 517 of the model parameters as well as the knowledge on the regions of the pa-  
 518 rameters space that are more likely to correspond to actual impedance mea-  
 519 surements, the problem becomes computationally treatable with a training  
 520 time that is lower than one minute for the GPR.

521 The three techniques, especially SVM and LS-SVM, have shown to be  
 522 more sensitive to noise than to the dataset size. Moreover, for very high  
 523 levels of noise, a big data set size has shown to be counterproductive. The  
 524 LS-SVM showed weaker results in terms of reconstruction error due to its  
 525 sensitivity to the hyperparameters' tuning and execution times similar to  
 526 the SVM. Therefore it can be considered a valuable option when a small and  
 527 noisy training set is available. Indeed, in the latter case the poor performance  
 528 of the three techniques are comparable and the simplicity of the method is  
 529 better exploited. The GPR and the SVM have shown very promising results  
 530 both in simulated and experimental environment. GPR has been able to  
 531 give an optimal reconstruction of the 45% of the spectra and a moderately  
 532 good reconstruction of a further 11%. SVR gives a slightly lower accuracy  
 533 that is compensated by the execution time required for the inference of the  
 534 parameters, which is almost halved with respect to the execution time of the  
 535 GPR.

## 536 Appendix A. Fouquet Equivalent Circuit Model

537 The Fouquet equivalent circuital model has already been adopted in  
 538 [21][36][2] for the identification of PEMFC operating in faulty conditions,  
 539 and it is defined as follows.

$$Z(f) = \bar{Z}_F(f; \mathbf{x}) = R_\Omega + \frac{\dot{Z}_{\text{CPE}}(\omega)(R_{\text{ct}} + \dot{Z}_{\text{W}}(\omega))}{\dot{Z}_{\text{CPE}}(\omega) + R_{\text{ct}} + \dot{Z}_{\text{W}}(\omega)}, \quad (\text{A.1})$$

540 with

$$\dot{Z}_{CPE}(f) = \frac{1}{Q(j\omega)^\phi}. \quad (\text{A.2})$$

$$\dot{Z}_W(f) = R_d \frac{\tanh \sqrt{j\omega\tau_d}}{\sqrt{j\omega\tau_d}}, \quad (\text{A.3})$$

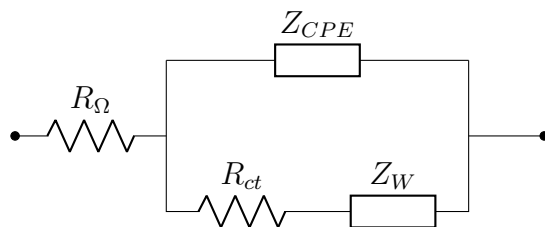


Figure A.8: The Fouquet equivalent circuit model.

541 Here  $\omega = 2\pi f$  is the angular frequency. The equivalent circuit model  
 542 makes use of a vector of  $N_p = 6$  parameters  $\mathbf{x} = [R_\Omega, R_{ct}, Q, \phi, R_d, \tau_d]^T$ .

543  $R_\Omega$  takes into account the losses due to the resistance of the electrolyte to  
 544 the flow of protons, while  $R_{ct}$  represents the resistance at the electrode/electrolyte  
 545 interface to the flow of charges.  $Q$  and  $\phi$  are the parameter of the Constant  
 546 Phase Element (CPE), used to model the frequency behaviour of the elec-  
 547 trodes with rough or porous surfaces. The Warburg element is defined by  
 548  $R_d$ , that models the losses due to reactants' diffusion. The time constant of  
 549 the diffusion process is specified with the parameter  $\tau_d$ . The model is evalu-  
 550 ated at the same frequencies where the EIS experiment was performed and  
 551  $N_f = 48$  impedance points have been obtained.

## 552 References

- 553 [1] Real operation pem fuel cells health-state monitoring and diagnosis  
 554 based on dc-dc converter embedded eis, Tech. rep., european H2020  
 555 project (2015).  
 556 URL <https://pemfc.health-code.eu/>
- 557 [2] G. Petrone, W. Zamboni, G. Spagnuolo, An interval arithmetic-  
 558 based method for parametric identification of a fuel cell equiv-  
 559 alent circuit model, Applied Energy 242 (2019) 1226 – 1236.  
 560 doi:<https://doi.org/10.1016/j.apenergy.2019.03.136>.  
 561 URL <http://www.sciencedirect.com/science/article/pii/S0306261919305446>

- 562 [3] Z. Fei, F. Yang, K.-L. Tsui, L. Li, Z. Zhang, Early prediction of battery  
563 lifetime via a machine learning based framework, *Energy* 225 (2021)  
564 120205. doi:<https://doi.org/10.1016/j.energy.2021.120205>.  
565 URL <https://www.sciencedirect.com/science/article/pii/S0360544221004540>
- 566 [4] Z. Chen, N. Shi, Y. Ji, M. Niu, Y. Wang, Lithium-ion batteries  
567 remaining useful life prediction based on bls-rvm, *Energy* 234 (2021)  
568 121269. doi:<https://doi.org/10.1016/j.energy.2021.121269>.  
569 URL <https://www.sciencedirect.com/science/article/pii/S0360544221015176>
- 570 [5] S. Son, S. Jeong, E. Kwak, J. hyeong Kim, K.-Y. Oh, In-  
571 tegrated framework for soh estimation of lithium-ion batter-  
572 ies using multiphysics features, *Energy* 238 (2022) 121712.  
573 doi:<https://doi.org/10.1016/j.energy.2021.121712>.  
574 URL <https://www.sciencedirect.com/science/article/pii/S0360544221019605>
- 575 [6] M. Zhang, T. Hu, L. Wu, G. Kang, Y. Guan, A method for  
576 capacity estimation of lithium-ion batteries based on adaptive  
577 time-shifting broad learning system, *Energy* 231 (2021) 120959.  
578 doi:<https://doi.org/10.1016/j.energy.2021.120959>.  
579 URL <https://www.sciencedirect.com/science/article/pii/S036054422101207X>
- 580 [7] C. Qian, B. Xu, L. Chang, B. Sun, Q. Feng, D. Yang, Y. Ren, Z. Wang,  
581 Convolutional neural network based capacity estimation using random  
582 segments of the charging curves for lithium-ion batteries, *Energy* 227  
583 (2021) 120333. doi:<https://doi.org/10.1016/j.energy.2021.120333>.  
584 URL <https://www.sciencedirect.com/science/article/pii/S036054422100582X>
- 585 [8] W.-Y. Lee, H. Oh, M. Kim, Y.-Y. Choi, Y.-J. Sohn, S.-G. Kim,  
586 Hierarchical fault diagnostic method for a polymer electrolyte fuel  
587 cell system, *International Journal of Hydrogen Energy* 45 (47)  
588 (2020) 25733 – 25746, special Issue on HYPOTHESIS XIV.  
589 doi:<https://doi.org/10.1016/j.ijhydene.2019.10.145>.  
590 URL <http://www.sciencedirect.com/science/article/pii/S0360319919339564>
- 591 [9] Z. Zhang, S. Li, Y. Xiao, Y. Yang, Intelligent simultane-  
592 ous fault diagnosis for solid oxide fuel cell system based on  
593 deep learning, *Applied Energy* 233-234 (2019) 930 – 942.  
594 doi:<https://doi.org/10.1016/j.apenergy.2018.10.113>.  
595 URL <http://www.sciencedirect.com/science/article/pii/S0306261918316854>

- 596 [10] D. Benouioua, D. Candusso, F. Harel, P. Picard, X. François, On the  
597 issue of the pemfc operating fault identification: Generic analysis tool  
598 based on voltage pointwise singularity strengths, *International Journal*  
599 *of Hydrogen Energy* 43 (25) (2018) 11606 – 11613, *alternative Energies*  
600 *for Sustainability*. doi:<https://doi.org/10.1016/j.ijhydene.2017.09.177>.  
601 URL <http://www.sciencedirect.com/science/article/pii/S0360319917338934>
- 602 [11] K. Chen, S. Laghrouche, A. Djerdir, Degradation model  
603 of proton exchange membrane fuel cell based on a  
604 novel hybrid method, *Applied Energy* 252 (2019) 113439.  
605 doi:<https://doi.org/10.1016/j.apenergy.2019.113439>.  
606 URL <http://www.sciencedirect.com/science/article/pii/S03606261919311134>
- 607 [12] K. Chen, S. Laghrouche, A. Djerdir, Proton exchange mem-  
608 brane fuel cell prognostics using genetic algorithm and ex-  
609 treme learning machine, *Fuel Cells* 20 (3) (2020) 263–271.  
610 arXiv:<https://onlinelibrary.wiley.com/doi/pdf/10.1002/fuce.201900085>,  
611 doi:<https://doi.org/10.1002/fuce.201900085>.  
612 URL <https://onlinelibrary.wiley.com/doi/abs/10.1002/fuce.201900085>
- 613 [13] R. Ma, T. Yang, E. Breaz, Z. Li, P. Briois, F. Gao, Data-driven  
614 proton exchange membrane fuel cell degradation predication through  
615 deep learning method, *Applied Energy* 231 (2018) 102 – 115.  
616 doi:<https://doi.org/10.1016/j.apenergy.2018.09.111>.  
617 URL <http://www.sciencedirect.com/science/article/pii/S03606261918314181>
- 618 [14] K. V. S. Bharath, F. Blaabjerg, A. Haque, M. A. Khan, Model-based  
619 data driven approach for fault identification in proton exchange mem-  
620 brane fuel cell, *Energies* 13 (12) (2020) 3144. doi:[10.3390/en13123144](https://doi.org/10.3390/en13123144).  
621 URL <http://dx.doi.org/10.3390/en13123144>
- 622 [15] H. Liu, J. Chen, D. Hissel, M. Hou, Z. Shao, A multi-  
623 scale hybrid degradation index for proton exchange mem-  
624 brane fuel cells, *Journal of Power Sources* 437 (2019) 226916.  
625 doi:<https://doi.org/10.1016/j.jpowsour.2019.226916>.  
626 URL <http://www.sciencedirect.com/science/article/pii/S0378775319309097>
- 627 [16] H. Liu, J. Chen, D. Hissel, H. Su, Remaining useful life  
628 estimation for proton exchange membrane fuel cells using  
629 a hybrid method, *Applied Energy* 237 (2019) 910 – 919.

- 630 doi:<https://doi.org/10.1016/j.apenergy.2019.01.023>.  
631 URL <http://www.sciencedirect.com/science/article/pii/S0306261919300236>
- 632 [17] B. Najafi, P. Bonomi, A. Casalegno, F. Rinaldi, A. Baricci, Rapid  
633 fault diagnosis of pem fuel cells through optimal electrochemi-  
634 cal impedance spectroscopy tests, *Energies* 13 (14) (2020) 3643.  
635 doi:[10.3390/en13143643](https://doi.org/10.3390/en13143643).  
636 URL <http://dx.doi.org/10.3390/en13143643>
- 637 [18] A. V. Pantelev, A. V. Lobanov, Mini-batch adaptive random  
638 search method for the parametric identification of dynamic sys-  
639 tems, *Automation and Remote Control* 81 (11) (2020) 2026 – 2045.  
640 doi:<https://doi.org/10.1134/S0005117920110065>.  
641 URL "<https://link.springer.com/article/10.1134%2FS0005117920110065>"
- 642 [19] Y. Bao, J. M. Velni, Data-driven linear parameter-varying model iden-  
643 tification using transfer learning, *IEEE Control Systems Letters* 5 (5)  
644 (2021) 1579–1584. doi:[10.1109/LCSYS.2020.3041407](https://doi.org/10.1109/LCSYS.2020.3041407).
- 645 [20] H. Kabir, L. Zhang, M. Yu, P. H. Aaen, J. Wood, Q.-J. Zhang, Smart  
646 modeling of microwave devices, *IEEE Microwave Magazine* 11 (3) (2010)  
647 105–118. doi:[10.1109/MMM.2010.936079](https://doi.org/10.1109/MMM.2010.936079).
- 648 [21] N. Fouquet, C. Doulet, C. Nouillant, G. Dauphin-Tanguy, B. Ould-  
649 Bouamama, Model based pem fuel cell state-of-health monitoring via  
650 ac impedance measurements, *Journal of Power Sources* 159 (2) (2006)  
651 905–913. doi:<https://doi.org/10.1016/j.jpowsour.2005.11.035>.  
652 URL <https://www.sciencedirect.com/science/article/pii/S0378775305015946>
- 653 [22] M. A. Kappel, R. Fabbri, R. P. Domingos, I. N. Bastos, Novel  
654 electrochemical impedance simulation design via stochastic algo-  
655 rithms for fitting equivalent circuits, *Measurement* 94 (2016) 344–354.  
656 doi:<https://doi.org/10.1016/j.measurement.2016.08.008>.  
657 URL <https://www.sciencedirect.com/science/article/pii/S0263224116304699>
- 658 [23] M. A. Abud Kappel, F. C. Peixoto, G. M. Platt, R. P. Domingos, I. N.  
659 Bastos, A study of equivalent electrical circuit fitting to electrochemical  
660 impedance using a stochastic method, *Applied Soft Computing* 50  
661 (2017) 183–193. doi:<https://doi.org/10.1016/j.asoc.2016.11.030>.  
662 URL <https://www.sciencedirect.com/science/article/pii/S1568494616305993>

- 663 [24] Z. Sun, D. Cao, Y. Ling, F. Xiang, Z. Sun, F. Wu, Proton exchange  
664 membrane fuel cell model parameter identification based on dynamic  
665 differential evolution with collective guidance factor algorithm, *Energy*  
666 216 (2021) 119056. doi:<https://doi.org/10.1016/j.energy.2020.119056>.  
667 URL <https://www.sciencedirect.com/science/article/pii/S0360544220321630>
- 668 [25] V. N. Vapnik, *The nature of statistical learning theory*, Springer-Verlag  
669 New York, Inc., 1995.
- 670 [26] J. A. K. Suykens, T. V. Gestel, J. D. Brabanter, B. D. Moor, J. Vande-  
671 walle, *Least Squares Support Vector Machines*, World Scientific, 2002.
- 672 [27] C. E. Rasmussen, C. K. I. Williams, *Gaussian Processes for Machine*  
673 *Learning*, MIT Press, 2006.
- 674 [28] R. Trincherio, M. Larbi, H. M. Torun, F. G. Canavero, M. Swaminathan,  
675 *Machine learning and uncertainty quantification for surrogate models of*  
676 *integrated devices with a large number of parameters*, *IEEE Access* 7  
677 (2019) 4056–4066.
- 678 [29] J.-M. Bourinet, *Reliability analysis and optimal design under uncer-*  
679 *tainty - Focus on adaptive surrogate-based approaches*, *Habilitation à*  
680 *diriger des recherches*, Université Clermont Auvergne (Jan. 2018).  
681 URL <https://tel.archives-ouvertes.fr/tel-01737299>
- 682 [30] P. Moçotéguy, B. Ludwig, D. Beretta, T. Pedersen, *Study*  
683 *of the impact of reactants utilization on the performance of*  
684 *pemfc commercial stacks by impedance spectroscopy*, *Internation-*  
685 *al Journal of Hydrogen Energy* 46 (10) (2021) 7475–7488.  
686 doi:<https://doi.org/10.1016/j.ijhydene.2020.11.197>.  
687 URL <https://www.sciencedirect.com/science/article/pii/S0360319920344475>
- 688 [31] P. Moçotéguy, B. Ludwig, D. Beretta, T. Pedersen, *Study*  
689 *of the impact of water management on the performance of*  
690 *pemfc commercial stacks by impedance spectroscopy*, *Internation-*  
691 *al Journal of Hydrogen Energy* 45 (33) (2020) 16724–16737.  
692 doi:<https://doi.org/10.1016/j.ijhydene.2020.04.139>.  
693 URL <https://www.sciencedirect.com/science/article/pii/S0360319920315421>
- 694 [32] T. Söderström, P. Stoica, *System identification*, New York (N.Y.) :  
695 Prentice-Hall, 1989.

- 696 [33] S. Boyd, S. P. Boyd, L. Vandenberghe, Convex optimization, Cambridge  
697 university press, 2004.
- 698 [34] B. Ghogh, M. Crowley, The theory behind overfitting, cross val-  
699 idation, regularization, bagging, and boosting: Tutorial (2019).  
700 arXiv:1905.12787.
- 701 [35] A. J. Smola, B. Schölkopf, A tutorial on support vector  
702 regression, *Statistics and Computing* 14 (3) (2004) 199–222.  
703 doi:10.1023/B:STCO.0000035301.49549.88.
- 704 [36] W. Zamboni, G. Petrone, G. Spagnuolo, D. Beretta, An evolutionary  
705 computation approach for the online/on-board identification of pem  
706 fuel cell impedance parameters with a diagnostic perspective, *Energies*  
707 12 (22) (2019). doi:10.3390/en12224374.  
708 URL <https://www.mdpi.com/1996-1073/12/22/4374>
- 709 [37] X. Yang, X. Cheng, Active learning method combining kriging model  
710 and multimodal-optimization-based importance sampling for the esti-  
711 mation of small failure probability, *International Journal for Numerical*  
712 *Methods in Engineering* 121 (21) (2020) 4843–4864.
- 713 [38] P. Agarwal, O. D. Crisalle, M. E. Orazem, L. H. Garcia-Rubio, Ap-  
714 plication of measurement models to impedance spectroscopy: II .  
715 determination of the stochastic contribution to the error structure,  
716 *Journal of The Electrochemical Society* 142 (12) (1995) 4149–4158.  
717 doi:10.1149/1.2048478.
- 718 [39] E. Brochu, V. M. Cora, N. de Freitas, A tutorial on bayesian optimiza-  
719 tion of expensive cost functions, with application to active user modeling  
720 and hierarchical reinforcement learning (2010). arXiv:1012.2599.
- 721 [40] E. A. Gouda, M. F. Kotb, A. A. El-Fergany, Jellyfish search algo-  
722 rithm for extracting unknown parameters of pem fuel cell models:  
723 Steady-state performance and analysis, *Energy* 221 (2021) 119836.  
724 doi:<https://doi.org/10.1016/j.energy.2021.119836>.  
725 URL <https://www.sciencedirect.com/science/article/pii/S0360544221000852>
- 726 [41] W. H. Tanveer, H. Rezk, A. Nassef, M. A. Abdelkareem, B. Kolosz,  
727 K. Karuppasamy, J. Aslam, S. O. Gilani, Improving fuel cell

- 728 performance via optimal parameters identification through fuzzy  
729 logic based-modeling and optimization, *Energy* 204 (2020) 117976.  
730 doi:<https://doi.org/10.1016/j.energy.2020.117976>.  
731 URL <https://www.sciencedirect.com/science/article/pii/S0360544220310835>
- 732 [42] Z. Yang, Q. Liu, L. Zhang, J. Dai, N. Razmjooy, Model pa-  
733 rameter estimation of the pemfcs using improved barnacles  
734 mating optimization algorithm, *Energy* 212 (2020) 118738.  
735 doi:<https://doi.org/10.1016/j.energy.2020.118738>.  
736 URL <https://www.sciencedirect.com/science/article/pii/S0360544220318454>
- 737 [43] E. A. Adinolfi, M. Gallo, P. Polverino, D. Beretta, S. S. Araya, C. Pi-  
738 anese, Ecm-based algorithm for on-board pemfcs diagnosis, in: W. Zam-  
739 boni, G. Petrone (Eds.), *ELECTRIMACS 2019*, Springer International  
740 Publishing, Cham, 2020, pp. 103–115.